

A New Approach in Material Modeling Towards Shear Cutting of Carbon Fiber Reinforced Plastics

L. Poggenpohl, S. Wulfinghoff, S. Reese

In this paper, a new approach in material modeling related to shear cutting of carbon fiber reinforced plastics (CFRP) is introduced. The aim is to formulate a phenomenological model accounting for the inner (micromechanical) processes which influence the cutting behavior and the quality of the cutting surface. This is required to make shear cutting of CFRP suitable for mass production like car manufacturing in terms of reduction of processing costs.

1 Introduction

In car manufacturing, especially when it comes to electric cars, weight reduction is one of the key possibilities to achieve a higher energy efficiency. But improvements in construction and design are somewhat limited. Carbon fiber reinforced plastics offer a possibility to reduce weight due to their high specific modulus and high specific strength. However, the drawback of CFRP are the high manufacturing and processing costs, which prevent them from being available for mass production. Since CFRP normally is produced near net shape (see Azmi (2012)), most processing is performed by drilling holes and milling the edges. If it is possible to substitute drilling and milling by punching and shear cutting, these processing costs could be reduced significantly.

Unfortunately there is not much knowledge about the inner processes (e.g. matrix/fiber cracking, debonding, ...) during shear cutting of CFRP. But this knowledge is crucial in order to understand and improve the shear cutting process and therefore to make it available for industrial mass production. To gain this knowledge, a new material approach based on experimental investigations is introduced in this paper and extended to a micromorphic model (Forest (2009)) as it is often used in gradient-extended damage and plasticity (e.g. Wulfinghoff et al. (2013b); Bayerschen et al. (2015); Ziemann et al. (2015)).

2 Ansatz for the Elastic Energy

In this section, an ansatz for the internal elastic energy will be proposed and compared to classical transversal isotropy. This ansatz is based on the assumption, that a sharp distinction between the carbon fibers with a high value of Young's modulus and strength and the epoxy resin with a low value of Young's modulus and strength is possible. Furthermore it is assumed, that the fibers can be treated as one dimensional geometries. Due to this assumption, and the restriction to unidirectional long fiber CFRP, a distinctive fiber direction can be introduced as it can be seen in Fig. 1.

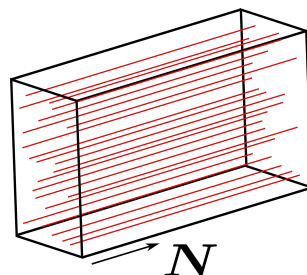


Figure 1: Visualization of the unidirectional long fiber CFRP. One-dimensional fibers are colored in red.

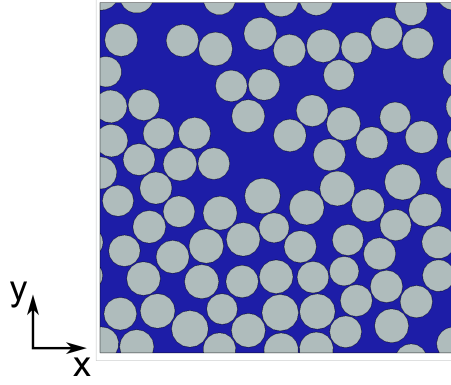


Figure 2: Exemplary geometry of the Repeating Unit Cell. Blue: matrix, gray: fibers.

| | Young's modulus [GPa] | Poisson's ratio [-] |
|--------|-----------------------|---------------------|
| Fiber | 240 | 0.23 |
| Matrix | 3.6 | 0.35 |

Table 1: List of material parameters for the RUC simulations.

2.1 Approach on the Internal Energy

Keeping the aforementioned assumptions in mind, one can obtain the internal energy using a simple extension of the isotropic elastic energy:

$$\psi = \psi_1(\boldsymbol{\varepsilon}) + \psi_2(\epsilon_f) = \frac{\lambda_1}{2} \text{tr}^2(\boldsymbol{\varepsilon}) + \mu_1 \text{tr}(\boldsymbol{\varepsilon}^2) + \frac{1}{2} E_2 \epsilon_f^2. \quad (1)$$

Here, E_2 represents the additional stiffness along the fiber direction. The elongation along the fibers is given by ϵ_f , which can be calculated by

$$\epsilon_f = \mathbf{N} \cdot (\boldsymbol{\varepsilon} \mathbf{N}). \quad (2)$$

As it can be seen in Eqs. (1) and (2), the standard isotropic energy has been extended by a part, where only the elongation along fiber normal direction contributes to the internal energy.

2.2 Comparison of standard transversal isotropic and new material model

The new approach was tested against the stiffness of a repeating unit cell (RUC). An isotropic and linear elastic material model was used for fiber and matrix (material parameters in table 1). The geometries for the RUC had been created based on a cross sectional image of a real CFRP ply. The average fiber volume fraction of all six RUCs hereby was 53.7%. After application of periodic boundary conditions and a far field strain, macroscopic stresses were calculated by volume averaging.

The average material stiffness tensor (in normalized Voigt notation) of all six RUCs takes the form

$$\mathbb{C}^{RUC} = \begin{bmatrix} 17.30 & 6.95 & 6.58 & 0 & 0 & 0 \\ 6.95 & 16.86 & 6.49 & 0 & 0 & 0 \\ 6.58 & 6.49 & 132.44 & 0 & 0 & 0 \\ 0 & 0 & 0 & 10.58 & 0 & 0 \\ 0 & 0 & 0 & 0 & 11.02 & 0 \\ 0 & 0 & 0 & 0 & 0 & 9.67 \end{bmatrix} \text{GPa}. \quad (3)$$

Please note, that some entries which were close to zero were assumed to be zero. It can be seen from Eq. (3) that the RUC-average is approximately transversely isotropic. A material stiffness tensor based on the previously shown approach was used to approximate \mathbb{C}^{RUC} . After approximation, the overall relative error is 0.64%. Keeping in mind the simplicity (use of only 3 Material parameters) of the new approach, the range of error (at least for this combination of materials) is considered acceptable.

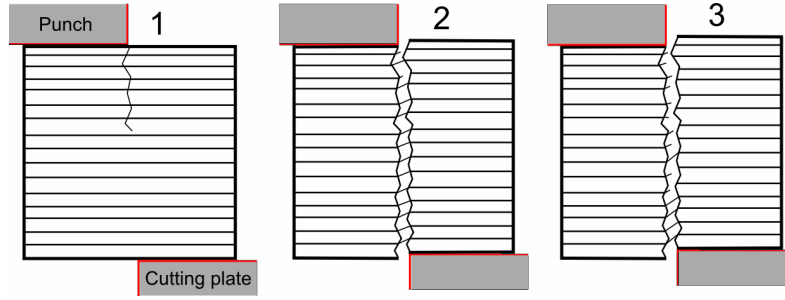


Figure 3: Visualization of the assumed process during shear cutting

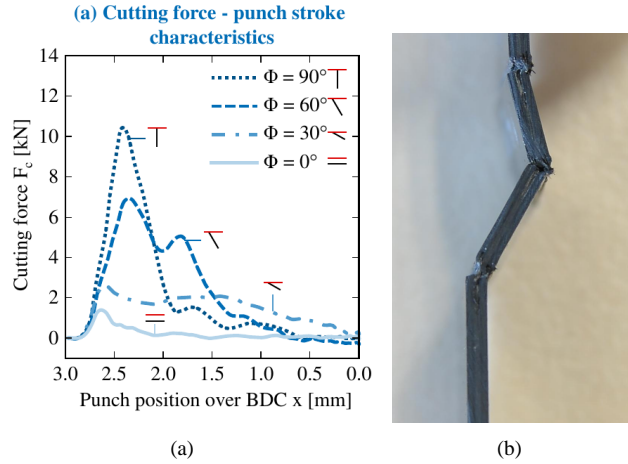


Figure 4: Experimental results: a) Cutting force over punch stroke (Shirobokov et al. (2015)), b) incomplete cut specimen after experiment.

3 Assumptions on the Micromechanical Processes

As it can be seen in Fig. 3, the shear cutting process can be assumed to be split in three phases. In phase one, after initiation of contact between work piece and punch and exceedance of the material strength of the matrix, a crack is propagating through the matrix material. In phase two, the bridging fibers get reoriented in the cutting plane and therefore start transmitting the cutting force. In phase three, the stresses in the fibers exceed the strength and the onset of fiber rupture starts the final separation process.

3.1 Comparison to Experimental Results

A good agreement of the assumptions made in the previous section and real processes can be seen in results of planking experiments of Shirobokov et al. (2015). In Fig. 4(a) the cutting forces over punch stroke from experiments of Shirobokov et al. (2015) are shown. While the cutting force is shown on the y -axis, the x -axis represents the position of the punch over the cutting plate. This means, that a value of 0 on the x -axis should indicate a fully separated material. As it will be shown later on, this does not hold for all specimens.

In Fig. 4(a) it can be seen, that the cutting force shows two peaks for several angles between fiber normal direction and cutting plane. The most distinctive peaks can be seen at an angle of 60° . These two peaks can be correlated to the stages in Fig. 3. At the first peak, matrix damage is assumed to occur, which reduces material stiffness with exceeding deformation (Fig. 3, stage 1). At the bottom between the two peaks, the fibers bridging the cutting plane are assumed to get reoriented. This leads to an increased material stiffness (Fig. 3, stage 2). At the second peak, fiber rupture occurs, which then leads to final decrease of material stiffness in the cutting plane (Fig. 3, stage 3).

In Fig. 4(b), an exemplary specimen after shear cutting is shown. One can see, that a complete separation in the matrix material occurred while the fibers only got separated in $2/3$ of the cross section. The plate therefore completely lost its bending stiffness and can be easily kinked and shifted, but hardly pulled, since the material stiffness in fiber direction still exists. This is in good agreement with the introduced model which predicts material stiffness only in fiber direction, when matrix material is not existent.

4 Two Surface Damage Model

The micromechanical and phenomenological observations, as described in section 3, lead to a damage formulation, which consists of two separate damage variables which should be used in a nonlocal formulation. The nonlocality is achieved by introducing damage variables D_1 and D_2 not as internal variables but as additional degrees of freedom. Here, the derivation follows similar lines as Wulfinghoff (2017) and is in contrast to derivations starting from the principle of virtual power (e.g. Bayerschen et al. (2015)). The damage variables of different material points have to communicate and therefore so called generalized contact forces Ξ_1 and Ξ_2 have to be introduced. Generalized contact forces and damage rates then contribute to the power of external forces in analogy to traction/body forces and displacement rates:

$$\mathcal{P}_{\text{ext}} = \int_{\partial V} (\mathbf{t} \cdot \dot{\mathbf{u}} + \Xi_1 \dot{D}_1 + \Xi_2 \dot{D}_2) dA + \int_V \mathbf{b} \cdot \dot{\mathbf{u}} dV \quad (4)$$

4.1 Generalized Lemma of Cauchy

A generalized formulation of Cauchy's lemma is applied to the generalized contact forces. In its original application, the lemma of Cauchy reads

$$\mathbf{t}_n = \boldsymbol{\sigma} \mathbf{n}. \quad (5)$$

In analogy to this, a generalized lemma of Cauchy can be introduced:

$$\Xi_{j,n} = \boldsymbol{\xi}_j \cdot \mathbf{n} \quad j = 1, 2. \quad (6)$$

This shows, that the scalar traction forces Ξ_j can be replaced by a scalar product of a generalized stress $\boldsymbol{\xi}_j$ and a normal vector.

4.2 Second Law of Thermodynamics

The dissipation \mathcal{D}_{tot} of a system can be expressed as

$$\mathcal{D}_{\text{tot}} = \mathcal{P}_{\text{ext}} - \dot{\Psi} \geq 0, \quad (7)$$

where $\Psi = \int_V \psi dV$ denotes the internal energy of the system. It is assumed that ψ is of the form

$$\psi = \hat{\psi}(\boldsymbol{\varepsilon}, D_1, D_2, \nabla D_1, \nabla D_2). \quad (8)$$

Inserting Eq. (4) into Eq. (7) and application of the generalized lemma of Cauchy (Eq. (6)) leads to

$$\mathcal{D}_{\text{tot}} = \int_{\partial V} \left((\boldsymbol{\sigma} \mathbf{n}) \cdot \dot{\mathbf{u}} + (\boldsymbol{\xi}_1 \cdot \mathbf{n}) \dot{D}_1 + (\boldsymbol{\xi}_2 \cdot \mathbf{n}) \dot{D}_2 \right) dA + \int_V (\mathbf{b} \cdot \dot{\mathbf{u}} - \dot{\psi}) dV \geq 0. \quad (9)$$

Application of Gauss' theorem, which is not discussed here, and the knowledge, that this inequality has to hold for arbitrary subsystems V , finally leads to the following representation of the dissipation density:

$$\mathcal{D} = \text{div}(\boldsymbol{\sigma} \dot{\mathbf{u}} + \boldsymbol{\xi}_1 \dot{D}_1 + \boldsymbol{\xi}_2 \dot{D}_2) + \mathbf{b} \cdot \dot{\mathbf{u}} - \dot{\psi} \geq 0. \quad (10)$$

Using the product rule and applying the dependencies of ψ on $\boldsymbol{\varepsilon}$, D_1 , D_2 , ∇D_1 and ∇D_2 , one obtains

$$\mathcal{D} = (\boldsymbol{\sigma} - \partial_{\boldsymbol{\varepsilon}} \psi) : \dot{\boldsymbol{\varepsilon}} + \sum_{i=1}^2 \left[(\text{div}(\boldsymbol{\xi}_i) - \partial_{D_i} \psi) \dot{D}_i + (\boldsymbol{\xi}_i - \partial_{\nabla D_i} \psi) \cdot \nabla \dot{D}_i \right] \geq 0. \quad (11)$$

Please note, that the quasi-static linear momentum balance $\text{div}(\boldsymbol{\sigma}) + \mathbf{b} = 0$ has been applied. If one now assumes, that no dissipation occurs, when damage is not evolving, the brackets in front of the terms $\dot{\boldsymbol{\varepsilon}}$ and $\nabla \dot{D}_i$ should vanish. This leads to the following equations:

$$\boldsymbol{\sigma} = \partial_{\boldsymbol{\varepsilon}} \psi \quad (12)$$

$$\boldsymbol{\xi}_i = \partial_{\nabla D_i} \psi. \quad (13)$$

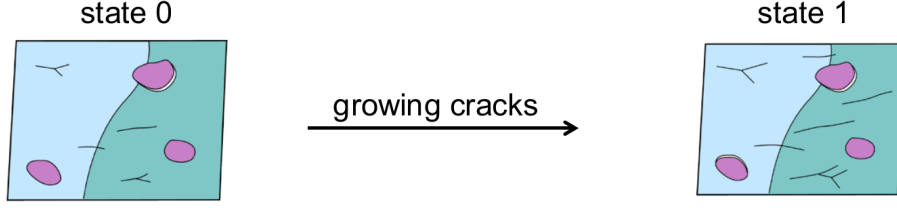


Figure 5: Motivation for the damage growth criterion of Wulfinghoff et al. (2017).

Finally, the reduced dissipation inequality reads

$$\mathcal{D} = \underbrace{(\operatorname{div}(\xi_1) - \partial_{D_1}\psi)}_{= Y_1} \dot{D}_1 + \underbrace{(\operatorname{div}(\xi_2) - \partial_{D_2}\psi)}_{= Y_2} \dot{D}_2 \geq 0. \quad (14)$$

Variables Y_1 and Y_2 can be interpreted as damage driving forces. In analogy to plasticity, damage criteria and evolution equations can be introduced for both damage variables:

$$f_i = Y_i - Y_{i,0}^c \leq 0, \quad \dot{D}_i \geq 0, \quad \dot{D}_i f_i = 0, \quad i = 1, 2 \quad (15)$$

Variable $Y_{i,0}^c$ in this case refers to the damage threshold in analogy to the yield surface in plasticity.

4.3 Damage Growth Criterion in Elastic Brittle Materials

Wulfinghoff et al. (2017) showed that the satisfaction of the second law of thermodynamics is not sufficient for phenomenological damage models, if the origin of damage are microscopic cracks. In addition, any constitutive model must satisfy an additional damage growth criterion in order to guarantee consistency with the microscopic picture of growing cracks (Fig. 5).

When damage is evolving in the sense of growing cracks, this reduces the internal mechanical energy. This reduction should hold not only for the applied strains, which led to the damage evolution, but also for arbitrary test strains. This should hold for arbitrary damage evolution, too. To summarize it in one sentence:

For every possible test strain, the stored mechanical energy in the system after damage evolution should be lower than in the system before damage evolution:

$$\psi(\tilde{\epsilon}, D) \geq \psi(\tilde{\epsilon}, D + dD) \quad \forall \tilde{\epsilon} \quad (16)$$

The damage growth criterion shown above guarantees, that damage will always lead to a loss of material stiffness. Scenarios, where the second law of thermodynamics is fulfilled, but damage leads to an increased material stiffness are prevented with this criterion. It can be shown easily that a formulation based on the energy

$$\psi = (1 - D_1) \left[\frac{\lambda_1}{2} \operatorname{tr}^2(\epsilon) + \mu_1 \operatorname{tr}(\epsilon^2) \right] + (1 - D_2) \frac{1}{2} E_2 \epsilon_f^2 + \psi_h(D_1, D_2) + \psi_g(\nabla D_1, \nabla D_2) \quad (17)$$

fulfills this damage growth criterion. Here, ψ_h denotes a damage hardening contribution (e.g. $\psi_h = K_h * D^2$) and ψ_g is gradient extension (e.g. $\psi_g = K_g * \nabla D^2$).

5 Conclusion and Outlook

A new material model to simulate the material behavior of CFRP was introduced. This material model is based on phenomenological assumptions. A comparison of the introduced model (with 3 elastic material parameters) and a RUC based material stiffness revealed a good agreement. A nonlocal damage formulation was derived in a thermodynamically consistent way, where the initial assumption of damage variables as additional degrees of freedom and conjugated contact forces formed the basis. It is stressed out, that only some minor assumption had to be done to derive all relations and equations necessary.

While the shown material model is derived in the regime of small deformations, in section 3 it is shown, that large rotations are expected to occur. Furthermore these finite rotations are a crucial part of material behavior in the cutting plane. For application to shear cutting, the material model would have to be generalized in the means of geometrical nonlinear theory (e.g. Saint-Venant-Kirchhoff material model).

A close investigation of the presented damage formulation reveals, that the second spatial derivative comes into play in Eq. (14):

$$\xi_i = \partial_{\nabla D_i} \psi \quad (18)$$

$$\Rightarrow Y_i = \operatorname{div}(\partial_{\nabla D_i} \psi) - \partial_{D_i} \psi. \quad (19)$$

To evaluate the damage criterion (15) based on this second derivative can be numerically difficult. A possibility to avoid this problem is the so called micromorphic extension which was introduced by Forest (2009). Here, a distinction between the local damage variable D and the global degree of freedom D^x with a coupling term

$$\psi_\chi = \frac{1}{2} H (D - D^x)^2 \quad (20)$$

is introduced. If the parameter H is chosen to be very high, the coupling of D and D^x is very stiff. In the extreme case

$$H \rightarrow \infty \quad \Rightarrow \quad D \rightarrow D^x \quad (21)$$

the previously introduced model is equivalent to the micromorphic model.

The micromorphic extension is not restricted to damage but may be applied to various inelastic models, e.g., plasticity (see, e.g., Wulfinghoff et al. (2013a)).

Acknowledgements

The financial support of the DFG Projects 'Scherschneiden kohlenstofffaserverstärkter Kunststoffe. Fertigungstechnologie und numerische Modellierung' (RE 1057/38-1) is gratefully acknowledged.

References

- Azmi, R. B. D., A.I.; Lin: *Tool wear prediction models during end milling of glass fibre-reinforced polymer composites* (2012).
- Bayerschen, E.; Stricker, M.; Wulfinghoff, S.; Weygand, D.; Böhlke, T.: Equivalent plastic strain gradient plasticity with grain boundary hardening and comparison to discrete dislocation dynamics. In: *Proc. R. Soc. A*, vol. 471, The Royal Society (2015).
- Forest, S.: Micromorphic approach for gradient elasticity, viscoplasticity, and damage. *Journal of Engineering Mechanics*, 135, 3, (2009), 117–131.
- Shirobokov, A.; Kerchnawe, S.; Terhorst, M.; Mattfeld, P.; Klocke, F.: Blanking of unidirectional carbon fibre reinforced plastics. *Applied Mechanics & Materials*, 794, (2015), 223–230.
- Wulfinghoff, S.: A generalized cohesive zone model and a grain boundary yield criterion for gradient plasticity derived from surface- and interface-related arguments. *International Journal of Plasticity*, 92, (2017), 57–78.
- Wulfinghoff, S.; Bayerschen, E.; Böhlke, T.: A gradient plasticity grain boundary yield theory. *International Journal of Plasticity*, 51, (2013a), 33–46.
- Wulfinghoff, S.; Bayerschen, E.; Böhlke, T.: Micromechanical simulation of the hall-petch effect with a crystal gradient theory including a grain boundary yield criterion. *PAMM*, 13, 1, (2013b), 15–18.
- Wulfinghoff, S.; Fassin, M.; Reese, S.: A damage growth criterion for anisotropic damage models motivated from micromechanics. *International Journal of Solids and Structures*, 121, (2017), 21–32.
- Ziemann, M.; Chen, Y.; Kraft, O.; Bayerschen, E.; Wulfinghoff, S.; Kirchlechner, C.; Tamura, N.; Böhlke, T.; Walter, M.; Gruber, P.: Deformation patterns in cross-sections of twisted bamboo-structured au microwires. *Acta Materialia*, 97, (2015), 216–222.